MOLECULAR PHYSICS, 1988, VOL. 64, NO. 3, 425–436

Infrared Fourier transform spectroscopy of XeH

by M. DOUAY, S. A. ROGERS† and P. F. BERNATH‡
Department of Chemistry, University of Arizona,
Tucson, Arizona 85721, U.S.A.

(*Received 22 January 1988; accepted 26 January 1988*)

The infrared emission spectrum of the Rydberg molecule XeH was recorded with the Kitt Peak Fourier transform spectrometer. XeH was made in a hollow cathode discharge of 2·2 torr H_2 and 0·1 torr Xe. The 0–0 bands of the $C\,^2\Pi$–$B\,^2\Sigma^+$ and the $D\,^2\Sigma^+$–$C\,^2\Pi$ transitions were observed near 3250 cm^{-1} and 4420 cm^{-1}, respectively. A rotational analysis provides spectroscopic constants for these states.

1. Introduction

More than 20 years ago, Michels and Harris [1] predicted the existence of bound excited states for the HeH molecule. This work, and more recent *ab initio* calculations on HeH [2–6], NeH [2, 7, 8] and ArH [2, 9–11], show that the excited states consist of an ionic core (HeH^+, NeH^+, ArH^+) and a Rydberg electron. In these 'Rydberg molecules' [12], the Rydberg electron contributes very little to the bonding, so the excited potential energy curves of the molecules closely resemble those of the corresponding ions. However, the ground $X\,^2\Sigma^+$ potential curves of the rare gas hydrides have only very shallow van der Waals minima.

The first observed electronic transition of a rare gas hydride molecule was reported by Johns in 1970 [13] for ArH. More recently, the spectra of HeH and NeH were reported in 1985 by Ketterle, Figger and Walther [14] and the spectra of KrH and KrD have been recorded for the first time by Dabrowski *et al.* [15]. In 1986 Lipson analysed transitions of XeH and XeD near 15000 cm^{-1} [16] in a Penning excitation source (Cossart lamp [17]). Additional observations on XeH and XeD have been made by Dabrowski, Herzberg and Lipson [18].

Brooks, Hunt and Miller [19–20] have published an account of a novel source for the production of HeH. They observed HeH emission spectra from the interface between helium gas and solid hydrogen when irradiated by a 15 MeV proton beam.

In addition to these bound-bound observations of rare gas hydrides, several groups have detected bound-free emission [21–22]. They observed ultraviolet emission from bound excited states to the repulsive wall of the shallow van der Waals ground state ($X\,^2\Sigma^+$).

The dissociation of HeH was also monitored by the detection of the neutral He and H fragments in charge-exchanged ion beam experiments [23–24]. Selgren and Gellene [25] have obtained some evidence for the metastability of ground state (or perhaps some excited state) of NeD.

† Present address: Department of Chemistry, University of Colorado, Boulder, Colorado 80309, U.S.A.
‡ Alfred P. Sloan Fellow; Camille and Henry Dreyfus Teacher-Scholar.

In the course of our work on the vibration-rotation spectrum of XeH^+ [26], we discovered two new infrared electronic transitions of XeH. A $^2\Pi$–$^2\Sigma^+$ transition near 3250 cm^{-1} and a $^2\Sigma^+$–$^2\Pi$ transition near 4420 cm^{-1} were assigned to Rydberg transitions of XeH.

2. Experimental

The experimental details are identical to those reported in the XeH^+ paper [26]. The XeH spectra were generated in a water-cooled nickel hollow cathode discharge lamp at a current of 200 mA. A slow, continuous flow of 2·2 torr hydrogen and 100 mtorr xenon was maintained through the lamp.

The molecular emission was recorded with the Fourier transform spectrometer associated with the McMath Solar Telescope of the National Solar Observatory at Kitt Peak. The 1800 cm^{-1}–5000 cm^{-1} region of the spectrum was recorded at 0·020 cm^{-1} resolution using liquid nitrogen cooled InSb detectors and a wedged Ge filter. The lower wavenumber limit was determined by the red limit of the detector, while the upper limit was set by the Ge filter.

Twenty scans were co-added in $1\frac{1}{2}$ hours of integration. The interferogram was Fourier transformed into a spectrum by G. Ladd of the National Solar Observatory.

3. Results

The XeH spectrum shows at least three transitions in the infrared, two of which were analysed. The spectrum was measured using a data reduction program developed at the National Solar Observatory called DECOMP. All lines were fitted by a non-linear least-squares procedure to Voigt lineshape functions.

Xe has nine stable isotopes: ^{124}Xe (0·1 per cent), ^{126}Xe (0·1 per cent), ^{128}Xe (1·9 per cent), ^{129}Xe (26·4 per cent), ^{130}Xe (4·1 per cent), ^{131}Xe (21·2 per cent), ^{132}Xe (26·9 per cent), ^{134}Xe (10·4 per cent), and ^{136}Xe (8·9 per cent). Unfortunately, the isotopic structure was usually only partly resolved and the lines were broadened by the presence of the different isotopes. For some R branch lines with $J > 20{\cdot}5$, the expected isotopic pattern begins to appear as shown in figure 1. However, not enough lines with a clear isotope effect were observed to warrant separate fits for each isotopomer. Consequently, our fits were performed with the strongest feature in the isotopic pattern. This feature is a blend of the lines of the ^{132}XeH and ^{131}XeH molecules. As a result, the line positions and constants obtained in our work will be close to those for ^{132}XeH and ^{131}XeH.

The signal-to-noise ratio for the strong lines was about 20 : 1. The relative line positions could be determined to a precision of about $\pm 0{\cdot}002$ cm^{-1}. The absolute calibration of $\pm 0{\cdot}001$ cm^{-1} was accomplished by observation of the vibration-rotation lines of OH [27] present as an impurity.

3.1. *The $C\,^2\Pi$–$B\,^2\Sigma^+$ transition*

This transition occurs at 3250 cm^{-1}. It shows strong Q_1, Q_2, R_1, R_2, P_1 and P_2 branches, but the spacing of adjacent lines of the Q_1 and Q_2 branches is very unusual for a $^2\Pi$–$^2\Sigma$ transition. As seen in figure 2, the Q_1 branch forms two heads, one at $J = 3{\cdot}5$ and one at $J = 13{\cdot}5$ due to the large γ value in the lower $^2\Sigma^+$ state (table 4).

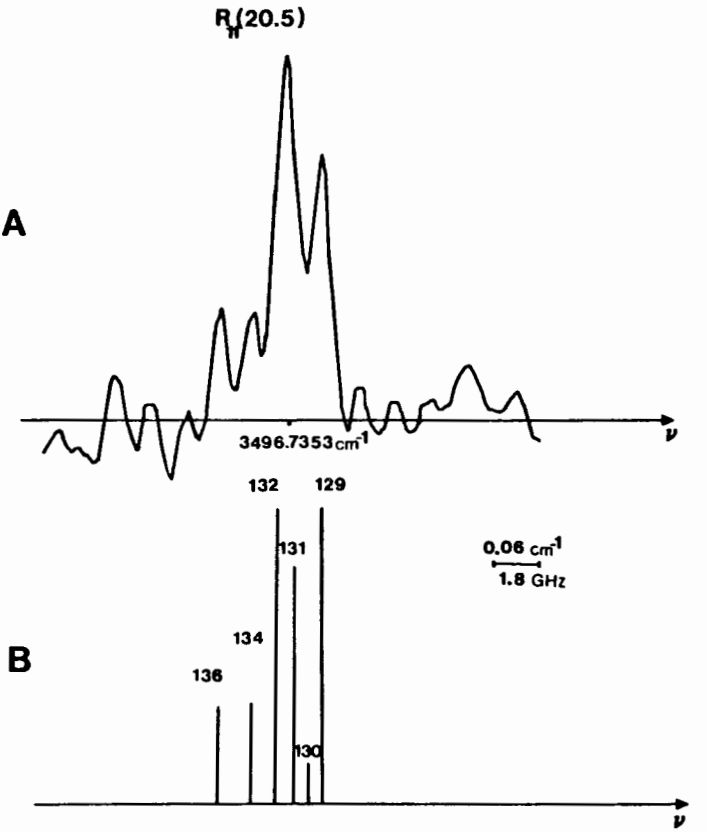

Figure 1. Panel *A* is the R_{11} (20·5) line of the 0–0 band of the $C\,^2\Pi$–$B\,^2\Sigma^+$ transition of XeH. The isotopic structure is just starting to be resolved. Panel *B* is a stick spectrum of the same transition with the masses of the various Xe isotopes indicated. In Panel *B*, the height of each line is proportional to the isotopic abundance, but the wavenumber scale is not real. The wavenumber scale was established by spacing the lines proportionally to their masses with the overall width of the pattern set by comparison with Panel *A*.

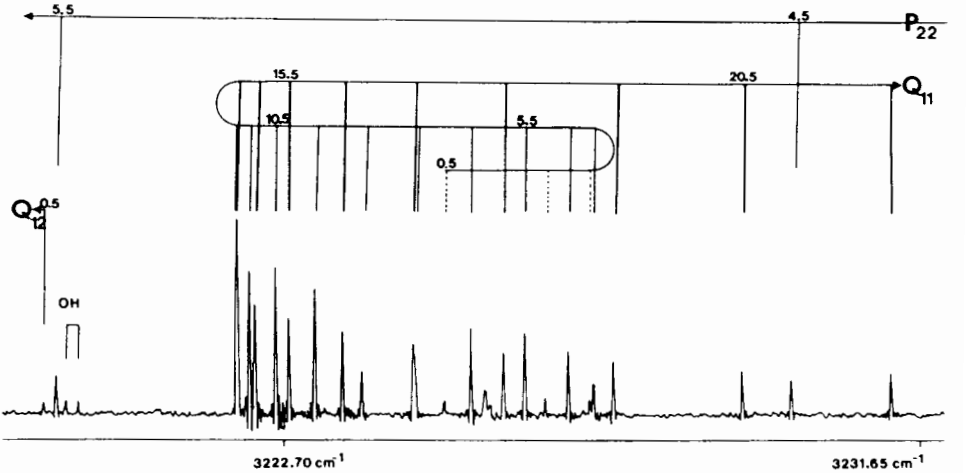

Figure 2. A portion of the 0–0 band of the $C\,^2\Pi$–$B\,^2\Sigma^+$ transition of XeH. Note the two band heads in the Q_{11} branch.

Table 1 (*a*).

Observed line positions of the $C\,^2\Pi$–$B\,^2\Sigma^+$ transition of XeH (in cm^{-1}).

J	P_{11}	O-C[a]	Q_{11}	O-C	R_{11}	O-C
0.5			3224.9056	0.0071[b]	3242.2503	0.0004
1.5	3208.1175	0.0032	3226.3202	0.0086[b]	3255.4294	0.0007
2.5	-	-	3226.9524	0.0024	3268.0509	-0.0022
3.5	3184.1681	-0.0029	3227.0045	0.0056	3280.2966	-0.0024
4.5	3171.3176	-0.0027	3226.6425	0.0026	3292.3095	-0.0027
5.5	3158.1312	-0.0030	3226.0280	0.0006	3304.2036	-0.0018
6.5	3144.7663	-0.0017	3225.2812	-0.0020	3316.0632	-0.0000
7.5	3131.3424	-0.0011	3224.4992	-0.0011	3327.9510	0.0024
8.5	3117.9551	0.0003	3223.7440	-0.0053	3339.9121	0.0037
9.5	3104.6747	0.0010	3223.0792	-0.0048	3351.9825	0.0042
10.5	3091.5560	-0.0005	3222.5420	-0.0041	3364.1870	0.0018
11.5	3078.6471	-0.0007	3222.1653	-0.0033	3376.5524	0.0023
12.5	3065.9866	0.0029[b]	3221.9773	-0.0005	3389.0878	-0.0015
13.5	-	-	3221.9936	-0.0018	3401.8144	-0.0013
14.5	3041.5017	-0.0021	3222.2436	0.0043	3414.7402	0.0008
15.5	3029.7343	-0.0008	3222.7291	0.0051	3427.8676	-0.0003
16.5	3018.3063	-0.0004	3223.4678	0.0060	3441.2079	0.0005
17.5	3007.2337	-0.0014	3224.4688	0.0061	3454.7628	0.0011
18.5	2996.5343	-0.0007	3325.7364	0.0019	3468.5348	0.0012
19.5	2986.2175	-0.0018	3227.2816	-0.0015	3482.5209	-0.0031
20.5	2976.2949	-0.0044[b]	3229.1073	-0.0051	3496.7353	0.0023
21.5	2966.7860	0.0012	3231.2171	-0.0073	3511.1608	0.0023
22.5	2957.6857	0.0015	3233.6147	-0.0041	3525.7961	-0.0014
23.5	2949.0045	0.0000	3236.3006	0.0074	3540.6446	-0.0009

a Observed-Calculated line positions computed with the constants of Tables 4 and 5.

b Blended line.

c Perturbed line.

Table 1 (*b*).

J	P_{22}	O-C	Q_{22}	O-C	R_{22}	O-C
0.5					3309.6500	0.0048[b]
1.5			3287.7867	-0.0024	3322.9640	0.0018
2.5	3253.2138	0.0027	3288.2676	-0.0009	3337.2797	0.0029
3.5	-	-	3289.7078	-0.0011	3352.4092	0.0040
4.5	3229.8002	0.0023	3291.9307	-0.0028	3368.1944	0.0027
5.5	3219.4507	0.0011	3294.7929	-0.0036	3384.5179	0.0036
6.5	3209.8056	0.0024	3298.1815	-0.0043	3401.2843	0.0040
7.5	3200.7474	0.0009	3302.0140	-0.0040	3418.4234	0.0032
8.5	3192.1968	0.0001	3306.2284	-0.0036	3435.8767	-0.0052
9.5	3184.0955	0.0010	3310.7809	-0.0021	3453.6201	-0.0059
10.5	3176.3969	-0.0007	3315.6381	0.0000	3471.6159	-0.0059
11.5	3169.0757	-0.0012	3320.7750	0.0022	3489.8407	-0.0052
12.5	3162.1110	-0.0009	3326.1728	0.0041	3508.2757	-0.0035
13.5	3155.4882	-0.0010	3331.8167	0.0048	3526.9044	-0.0022
14.5	3149.1989	-0.0011	3337.6972	0.0055	3545.7155	-0.0022
15.5	3143.2397	0.0003	3343.8030	0.0036	3564.6997	0.0038
16.5	3137.6070	0.0019	3350.1281	0.0001	3583.8418	0.0039
17.5	3132.2984	0.0016	3356.6687	-0.0025	3603.1382	0.0045
18.5	3127.3166	0.0010	3363.4162	-0.0073	3622.5789	0.0030
19.5	3122.6660	0.0024	3370.3732	-0.0062	3642.1575	0.0004
20.5	3118.3468	0.0032	3377.5285	-0.0045	3661.8680	-0.0022
21.5	3114.3492	-0.0093[b]	3384.8870	0.0089	3681.7063	-0.0017
22.5	3110.7085	-0.0030	-	-	-	-
23.5					3721.7233	-0.0019
24.5					3741.8815	-0.0051
25.5					3762.1416	0.0054

Table 1 (*c*).

J	Q_{12}	O-C	Q_{21}	O-C	R_{21}	O-C	R_{12}	O-C
0.5	3219.2761	0.0007			3314.9489	-0.0037[b]		
1.5	3215.0869	0.0005	3298.4867	0.0026	3333.5395	-0.0020		
2.5	3210.1568	0.0011	-	-	3353.0882	-0.0040		
3.5	3204.6708	0.0009	3311.2918	-0.0003	3373.4289	0.0010		
4.5	3198.8040	-0.0007	3319.0553	-0.0002	3394.4022	-0.0003	3266.7087	0.0108[c]
5.5	3192.7060	-0.0002	3327.5243	0.0031	3415.8974	-0.0064[c]	3273.2256	0.0041[c]
6.5	3186.4859	-0.0015	3336.5787	0.0027[c]	3437.8498	0.0021[c]		
7.5	3180.2344	0.0007	3346.1421	0.0057[c]	-	-		
8.5	3174.0098	0.0010	3356.1472	0.0058[c]	3482.8155	-0.0144[c]		
9.5	3167.8607	-0.0007	-	-				
10.5	3161.8295	0.0004	3377.3228	0.0017[c]				
11.5	3155.9404	-0.0006						
12.5	3150.2181	-0.0032[b]						

Table 2(*a*).

Observed transitions of the $D\,^2\Sigma^+ - C\,^2\Pi$ transition of XeH (in cm^{-1}).

J	P_{11}	O-C[a]	Q_{11}	O-C	R_{11}	O-C
0.5			4450.0190	0.0372		
1.5	4432.6428	0.0124	4444.9539	0.0219[c]		
2.5	4415.8476	0.0327[c]	4440.7498	0.0459[c]	4480.0086	0.0650[c]
3.5	4399.6559	0.0552[c]	4437.1760	0.0602[c]	4489.3667	0.0576[c]
4.5	4383.8848	0.0692[c]	4434.0416	0.0520[c]	4499.0987	0.0320[c]
5.5	4368.3747	0.0575[c]	4431.2055	0.0320[c]	4509.0745	0.0109[c]
6.5	4353.0288	0.0333[c]	4428.5602	0.0118[c]	4519.1751	-0.0045
7.5	4337.7793	0.0109[c]	4426.0234	0.0005	4529.3126	-0.0097
8.5	4322.5686	-0.0061[c]	4423.5227	-0.0050	4539.4096	-0.0103
9.5	4307.3561	-0.0125	4421.0076	-0.0020	4549.4087	-0.0076
10.5	4292.1030	-0.0124	4418.4290	0.0021	4559.2635	-0.0026
11.5	4276.7850	-0.0028	4415.7519	0.0065	4568.9356	0.0043
12.5	4261.3695	0.0056	4412.9455	0.0084	4578.3791	-0.0001
13.5	4245.8314	0.0058	4409.9872	0.0096		
14.5	4230.1696	0.0122	4406.8539	0.0085		
15.5	4214.3561	0.0107	4403.5236	0.0028		
16.5	4198.3760	-0.0008	4399.9822	-0.0032		
17.5	4182.2399	0.0000	4396.2143	-0.0075		
18.5	4165.9206	-0.0021	4392.2065	-0.0066		
19.5	-	-	4387.9319	-0.0110		
20.5	-	-	4383.4061	0.0110		

a Observed-Calculated line positions computed with the constants of Tables 5 and 6.

b Blended line.

c Perturbed line.

Table 2(*b*).

J	P_{22}	O-C	Q_{22}	O-C	R_{22}	O-C
1.5	4372.6183	-0.0141	4398.2341	-0.0056	4436.6248	0.0271
2.5	4363.0524	-0.0143	4401.5358	-0.0043	4452.6134	-0.0042
3.5	4352.5249	-0.0070	4403.9029	0.0006	4467.6313	-0.0016
4.5	4341.2014	-0.0047	4405.5016	0.0044	4481.8056	-0.0057[c]
5.5	4329.2360	-0.0031	4406.4663	0.0019[c]	4495.2647	-0.0272[c]
6.5	4316.7397	-0.0069[c]	4406.8872	-0.0220[c]	4508.1020	-0.0776[c]
7.5	4303.7845	-0.0303[c]	4406.8872	-0.0208[c]	-	-
8.5	4290.3729	-0.1329[c]	4406.7795	0.2652[c]	4532.5889	0.1357[c]
9.5	4277.2251	0.3607[c]	4405.9045	0.1399[c]	4544.0125	0.0891[c]
10.5	4263.0695	0.1479[c]	4404.7730	0.0900[c]	4555.0394	0.0589[c]
11.5	4248.7868	0.0876[c]	4403.3427	0.0580[c]	4565.6682	0.0339[c]
12.5	4234.2809	0.0694[c]	4401.6059	0.0283	4575.9011	0.0136
13.5	4219.4818	0.0147	4399.5713	0.0065		
14.5	4204.4766	0.0066	4397.2330	-0.0118		
15.5	-	-	4394.5857	-0.0277		
16.5	-	-	4391.6383	-0.0250		
17.5	-	-	4388.3766	-0.0084		
18.5	-	-	4384.7910	0.0235		

Table 2(*c*).

J	Q_{12}	O-C	Q_{21}	O-C	P_{12}	O-C	R_{12}	O-C	R_{21}	O-C
0.5									4488.2743	-0.0196
1.5	4372.7890	0.0295[c]			4359.9390	0.0114			4508.7548	-0.0153
2.5	4363.3319	0.0550[c]	4479.6533	0.0003	4337.7422	0.0402[c]	4401.8987	0.0680[c]	4530.0329	-0.0116
3.5	4352.8907	0.0682[c]	4488.9476	0.0062	4314.6190	0.0574[c]	4404.3304	0.0604[c]	4551.9193	-0.0069
4.5	4341.6304	0.0566[c]	4498.6259	-0.0000	4290.7617	0.0749[c]	4405.9731	0.0352[c]	4574.2169	-0.0101
5.5	4329.7099	0.0301[c]	4508.5530	-0.0016[c]	4266.2959	0.0691[c]	4406.9947	0.0214[c]		
6.5	4317.2692	0.0136[c]	4518.5797	-0.0279[c]	4241.3375	0.0404[c]	4407.4840	0.0027		
7.5	4304.3799	-0.0069	4528.5617	-0.1307[c]	4215.9910	0.0070[c]	4407.5366	-0.0012		
8.5	4291.1269	-0.0088	4538.9872	0.2496[c]	4190.3518	0.0003	4407.1976	0.0008		
9.5	4277.5357	-0.0110	4548.8213	0.1352[c]						
10.5	4263.6513	-0.0005	4558.5934	0.1013[c]						
11.5	4249.4674	-0.0058								

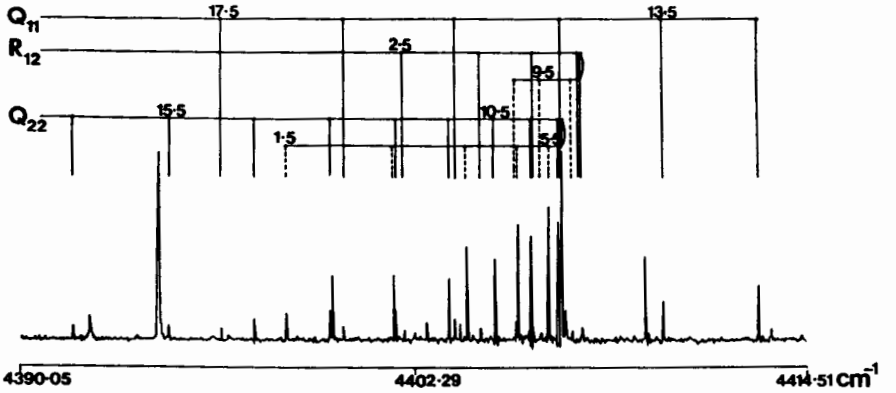

Figure 3. A portion of the 0–0 band of the $D\,^2\Sigma^+$–$C^2\Pi$ transition of XeH.

As predicted by Earls [28] for a $^2\Pi$ state in an intermediate Hund's case ($\lambda = A/B \approx 13$), the most intense branches are Q_1, Q_2, R_1, R_2, P_1, and P_2 and the satellite branches, Q_{12}, Q_{21}, R_{12}, R_{21}, P_{12}, and P_{21} branches are weaker. As expected, we saw the six main branches, but only four of the satellite branches (table 1). The P_{21} and P_{12} branches were too weak to be identified (table 1).

3.2. *The $D\,^2\Sigma^+$–$C\,^2\Pi$ transition*

The second transition near 4420 cm^{-1} has the appearance of a normal $^2\Sigma^+$–$^2\Pi$ transition (figure 3). The $^2\Pi$ state was found to be the same $^2\Pi$ state that was involved in the first transition near 3250 cm^{-1}. The six main branches were observed, along with five of the six weaker satellite branches (table 2). Only the P_{21} branch was not identified.

The upper $^2\Sigma^+$ state was found to be the upper state of the $^2\Sigma^+$–$^2\Sigma^+$ transition observed by Lipson [16]. In agreement with Lipson, we found this state to be perturbed at $J = 7{\cdot}5$ for the f parity component ($N = 8$, F_2). A slight shift of the e parity line at $J = 3{\cdot}5$ ($N = 3$, F_1) for the upper $^2\Sigma^+$ state was also present. No extra lines involving the perturbing state were identified in the spectrum, so a deperturbation analysis was not attempted.

Figure 4 is an energy level diagram of the known low-lying states of XeH. The $D\,^2\Sigma^+$–$A\,^2\Sigma^+$ near 15 000 cm^{-1} was observed by Lipson, while our two infrared transitions, $D\,^2\Sigma^+$–$C\,^2\Pi$ and $C\,^2\Pi$–$B\,^2\Sigma^+$ casade from the $D\,^2\Sigma^+$ state. The names of these electronic states are somewhat tentative since additional low-lying states are possible.

A simultaneous, weighted, non-linear least-squares fit of all of the lines of the combined $D\,^2\Sigma^+$–$C\,^2\Pi$–$B\,^2\Sigma^+$ transitions was carried out. The hamiltonian matrix for each state was derived with Hund's case (a) basis functions and diagonalized to produce the energy levels. The effective hamiltonian matrix of Brown *et al.* [29] was utilized. An explicit listing of the $^2\Pi$ matrix elements is provided in Table II of a paper by Amiot *et al.* [30]. It was necessary to derive one additional matrix element, p_L

$$2,2 \quad \mp 0{\cdot}5\,(z^2 + 8z + 8)(J + 0{\cdot}5)^3,$$

$$1,2 \quad \pm 0{\cdot}25\,z^{0{\cdot}5}\,(3z + 4)(J + 0{\cdot}5)^3,$$

where the definitions of Amiot *et al.* [30] are retained.

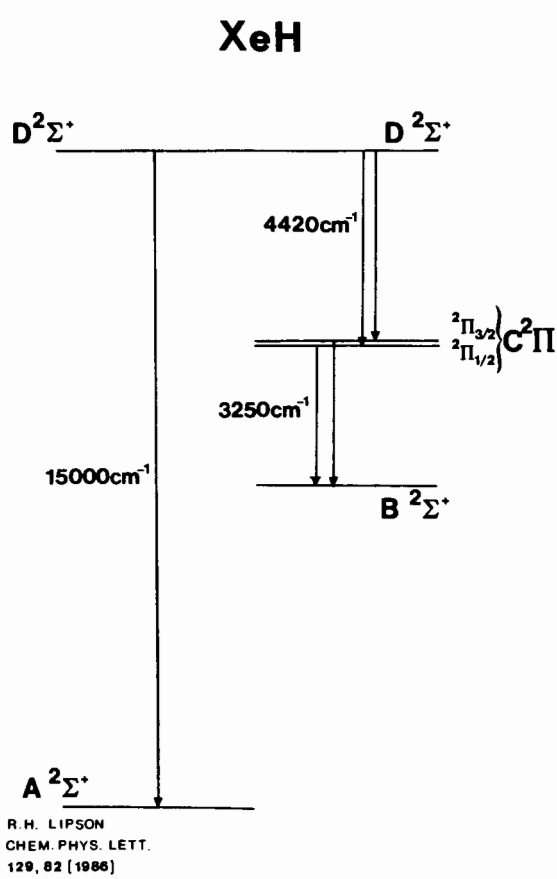

Figure 4. The low-lying states of XeH.

The $^2\Sigma^+$ matrix elements are also provided in Amiot *et al.*s paper [30], but we disagree with their matrix elements for γ, γ_D and γ_H. For the customary spin–rotation hamilton:

$$\hat{H}_{SR} = \hat{\mathbf{N}} \cdot \hat{\mathbf{S}} \, (\gamma + \gamma_D \hat{\mathbf{N}}^2 + \gamma_H \hat{\mathbf{N}}^4 + \gamma_L \hat{\mathbf{N}}^6)$$

the correct matrix elements are provided in table 3.

The spectroscopic parameters resulting from our fit of the lines of tables 1 and 2 are provided in tables 4, 5 and 6. Blended lines and perturbed lines were included in the final fit, but with reduced weights.

Table 3. Hamiltonian matrix elements for $a\,^2\Sigma^+$ state in a case (*a*) parity basis set.

T	e	1	γ	e	$+0{\cdot}5\,(J-0{\cdot}5)$
	f	1		f	$-0{\cdot}5\,(J+1{\cdot}5)$
B	e	$(J+0{\cdot}5)(J-0{\cdot}5)$	γ_D	e	$+0{\cdot}5\,(J-0{\cdot}5)^2(J+0{\cdot}5)$
	f	$(J+0{\cdot}5)(J+1{\cdot}5)$		f	$-0{\cdot}5\,(J+1{\cdot}5)^2(J+0{\cdot}5)$
D	e	$-[(J+0{\cdot}5)(J-0{\cdot}5)]^2$	γ_H	e	$+0{\cdot}5\,(J-0{\cdot}5)^3(J+0{\cdot}5)^2$
	f	$-[(J+0{\cdot}5)(J+1{\cdot}5)]^2$		f	$-0{\cdot}5\,(J+1{\cdot}5)^3(J+0{\cdot}5)^2$
H	e	$[(J+0{\cdot}5)(J-0{\cdot}5)]^3$	γ_L	e	$+0{\cdot}5\,(J-0{\cdot}5)^4(J+0{\cdot}5)^3$
	f	$[(J+0{\cdot}5)(J+1{\cdot}5)]^3$		f	$-0{\cdot}5\,(J+1{\cdot}5)^4(J+0{\cdot}5)^3$

Table 4. Spectroscopic constants (in cm^{-1}) for the $B\,^2\Sigma^+$ state of XeH.

T_{00}	7324·0398(29)†
B_0	6·386970(54)
$D_0 \times 10^4$	1·9974(20)
$H_0 \times 10^{10}$	4·4(22)
γ_0	7·44405(31)
$\gamma_{D_0} \times 10^3$	−1·6622(39)
$\gamma_{H_0} \times 10^7$	4·96(13)
$\gamma_{L_0} \times 10^{11}$	−6·4(15)

† The numbers in parentheses are one standard deviation in the last digit.

Table 5. Spectroscopic constants (in cm^{-1}) for the $C\,^2\Pi$ state of XeH.

T_{00}	10 576·9827(28)†
A_0	81·6977(15)
B_0	6·492172(54)
$D_0 \times 10^4$	1·8013(20)
$H_0 \times 10^9$	−9·64(21)
γ_0	0·32492(42)
$\gamma_{D_0} \times 10^4$	−1·777(35)
$\gamma_{H_0} \times 10^8$	8·36(50)
q_0	0·010860(24)
$q_{D_0} \times 10^6$	−1·58(14)
$q_{H_0} \times 10^9$	4·07(19)
p_0	0·26934(42)
$p_{D_0} \times 10^4$	−2·024(51)
$p_{H_0} \times 10^7$	2·74(18)
$p_{L_0} \times 10^{10}$	−1·12(20)

† The numbers in parentheses are one standard deviation in the last digit.

Table 6. Spectroscopic constants (in cm^{-1}) for the $D\,^2\Sigma^+$ state of XeH.

Constants	This work	Lipson
T_{00}	14 998·921†	14 998·921(13)‡
B_0	6·40766(10)	6·40776(48)
$D_0 \times 10^4$	2·1477(58)	2·208(29)
$H_0 \times 10^9$	−9·96(95)	
γ_0	0·08505(89)	0·0860(30)
$\gamma_{D_0} \times 10^4$	−1·735(84)	
$\gamma_{H_0} \times 10^7$	2·96(18)	

† Fixed to Lipson's value [18].
‡ The numbers in parentheses are one standard deviation in the last digit.

4. Discussion

In our experiment, XeH was produced in an electrical discharge, but the chemistry of a xenon and hydrogen plasma is different from that of the other rare gases plus hydrogen plasmas. As discussed in the XeH^+ paper [26], an excess of H_2 provides the most favourable conditions for XeH production. XeH was not observed when 1·2 torr of Xe and 0·02 torr of H_2 were used in our hollow cathode discharge. When an excess of hydrogen is present, H_3^+ is the dominant ion in the

discharge and will transfer a proton to Xe to produce XeH^+. The XeH^+ ion then captures an electron to form excited XeH. The XeH cools by cascade emission of radiation and eventually dissociates into Xe and H atoms.

As expected, there is good agreement between the observed spectroscopic constants of XeH (tables 4–6) and the corresponding values for XeH^+ [26]. Unfortunately, only 0–0 bands were observed for XeH, so vibrational constants and equilibrium molecular constants could not be derived.

For the $B\,^2\Sigma^+$ transition (figure 4), a spin–rotation constant, γ, of $7{\cdot}44\,cm^{-1}$ (table 4) was observed. Such a large value (greater than B) allowed the constants γ_D, γ_H and γ_L to be determined. A large γ value for a $^2\Sigma^+$ state suggests that a $^2\Pi$ state is nearby, but this state was not directly observed. A simple pure precession estimate ($l = 1$, $A = 60\,cm^{-1}$) indicates that the missing $B'\,^2\Pi$ state is about $200\,cm^{-1}$ above the $B\,^2\Sigma^+$ state. A few weak branches could be picked out near $3200\,cm^{-1}$, but analysis was not possible.

In keeping with spectroscopic custom, we have labelled the low-lying XeH states as $X\,^2\Sigma^+$, $A\,^2\Sigma^+$, $B\,^2\Sigma^+$, $C\,^2\Pi$ and $D\,^2\Sigma^+$. Our work on the $D\,^2\Sigma^+$ and $C\,^2\Pi$ states is in agreement with, but more accurate than, the previous analyses [16, 18]. The discovery of the $B\,^2\Sigma^+$ state and the indirect evidence for a $B'\,^2\Pi$ state represents our main contribution to the spectroscopy of XeH. We have resisted the temptation to assign atom nl quantum numbers to the Rydberg states of XeH. We suspect that n and l are probably poor quantum numbers for the A, B, C and D states of XeH and some *ab initio* theoretical guidance would be very helpful.

The National Solar Observatory is operated by the Association for Research in Astronomy, Inc., under contract with the National Science Foundation. We thank J. Wagner for technical assistance in acquiring the spectra. This research was supported by the Air Force Astronautics Laboratory (F 04611-87-K-0020).

References

[1] Michels, H. H., and Harris, F. E., 1963, *J. chem. Phys.*, **39,** 1464.
[2] Theodorakopoulos, G., Farantos, S. C., Buenker, R. J., and Peyerimhoff, S. D., 1984, *J. Phys.* B, **17,** 1453.
[3] Theodorakopoulos, G., Petsalakis, I. D., Nicolaides, C. A., and Buenker, R. J., 1987, *J. Phys.* B, **20,** 2339.
[4] Miller, W. H., and Schaefer III, H. F., 1970, *J. chem. Phys.*, **53,** 1421.
[5] Kubach, C., Sidis, V., Fussen, D., and van der Zande, W. J., 1987, *Chem. Phys.*, **117,** 439.
[6] Petsalakis, I. D., Theodorakopoulos, G., Nicolaides, C. A., and Buenker, R. J., 1987, *J. Phys.* B, **20,** 5959.
[7] Raynor, S., and Herschback, D. R., 1982, *J. phys. Chem.*, **86,** 3592.
[8] Theodorakopoulos, G., Petsalakis, I. D., and Buenker, R. J., 1987, *J. Phys.* B, **20,** 5335.
[9] Berman, M., Kaldor, U., Shmulovich, J., and Yatsiv, S., 1981, *Chem. Phys.*, **63,** 165.
[10] Vance, R. L., and Gallup, G. A., 1980, *J. chem. Phys.*, **73,** 894.
[11] van Hermert, M. C., Dohmann, H., and Peyerimhoff, S. D., 1986, *Chem. Phys.*, **110,** 55.
[12] Herzberg, G., 1987, *A. Rev. phys. Chem.*, **38,** 27.
[13] Johns, J. W. C., 1970, *J. molec. Spectrosc.*, **36,** 488.
[14] Ketterle, W., Figger, H., and Walther, H., 1985, *Phys. Rev. Lett.*, **55,** 2941.
[15] Dabrowski, I., Herzberg, G., Hurley, B. P., Lipson, R. H., Vervloet, M., and Wang, D. C., 1987, *Molec. Phys.*, **63,** 269.
[16] Lipson, R. H., 1986, *Chem. Phys. Lett.*, **129,** 82.

[17] COSSART, D., COSSART-MAGOS, C., GANDARA, G., and ROBBE, J. M., 1985, *J. molec. Spectrosc.*, **109,** 166.
[18] DABROWSKI, I., HERZBERG, G., and LIPSON, R. H., 1987, *Molec. Phys.*, **63,** 289.
[19] BROOKS, R. L., HUNT, J. L., and MILLER, J. J., 1987, *Phys. Rev. Lett.*, **58,** 199.
[20] BROOKS, R. L., and NICKEL, B. G., 1987, *Chem. Phys. Lett.*, **139,** 503.
[21] MOLLER, T., BELAND, M., and ZIMMER, G., 1985, *Phys. Rev. Lett.*, **55,** 2145; 1987 *Chem. Phys. Lett.*, **136,** 551.
[22] KETTERLE, W., DODHY, A., and WALTHER, H., 1986, *Phys. Rev. Lett.*, **129,** 76.
[23] PETERSON, J. R., and BAE, Y. K., 1986, *Phys. Rev.* A, **34,** 3517.
[24] VAN DER ZANDE, W. J., KOOT, W., DE BRUIJN, D. P., and KUBACH, C., 1986, *Phys. Rev. Lett.*, **57,** 1219.
[25] SELGREN, S. F., and GELLENE, G. I., 1987, *Chem. Phys. Lett.*, **141,** 508.
[26] ROGERS, S. A., BRAZIER, C. R., and BERNATH, P. F., 1987, *J. chem. Phys.*, **87,** 159.
[27] AMANO, T., 1984, *J. molec. Spectrosc.*, **103,** 436.
[28] EARLS, L. T., 1935, *Phys. Rev.*, **48,** 423.
[29] BROWN, J. M., COLBOURN, E. A., WATSON, J. K. G., and WAYNE, F. D., 1979, *J. molec. Spectrosc.*, **74,** 294.
[30] AMIOT, C., MAILLARD, J. P., and CHAUVILLE, J., 1981, *J. molec. Spectrosc.*, **87,** 196.